Journal of Applied Electrochemistry **34**: 659–669, 2004.

Reviews in Applied Electrochemistry. Number 55

Electrochemical corrosion behaviour of 90–10 Cu–Ni alloy in chloride-based electrolytes

G. KEAR[1]*, B.D. BARKER[2], K. STOKES[3] and F.C. WALSH[4]
[1]*C/o BRANZ Ltd, Materials Section, Science and Engineering Services, Private Bag 50 908, Porirva, New Zealand*
[2]*Applied Electrochemistry Group, University of Portsmouth PO1 2DT, Great Britain*
[3]*DSTL Winfrith, Winfrith Technology Park, Dorchester, DT2 8WX, Great Britain*
[4]*Electrochemical Engineering Group, Department of Chemical Engineering, University of Bath BA2 7AY, Great Britain*
*(*author for correspondence, e-mail: garethkear@hotmail.com)*

Received 9 July 2003; accepted in revised form 26 January 2004

Key words: 90–10 copper–nickel, corrosion, NaCl, oxygen reduction, RCE, RDE, seawater

Abstract

The corrosion of 90–10 copper–nickel alloy in aqueous chloride electrolytes has received considerable attention in the literature due to its widespread use in seawater and saline environments. From an analysis of the electrochemical behaviour of the alloy, it is clear that both the polarization and mixed/corrosion potential characteristics show a close comparison to unalloyed copper. Important differences arise, however, due to the semi–conducting nature, composition and overall protectiveness of the corrosion products on the 90–10 copper–nickel alloy. In this work the metallurgy, electrochemistry and mechanism of passivation of the alloy are reviewed to provide a focused source of data regarding the electrochemical characteristics of the alloy in saline media.

1. Introduction

Copper-based alloys are among the most important commercial metals in the marine environment due to their excellent electrical and thermal conductivities, good corrosion resistance and ease of manufacture [1]. The copper–nickel–iron alloys were first developed during World War II as a replacement to copper in Royal Navy seawater pipework [2]. The 90–10 copper–nickel composition generally chosen for production has a nominal composition of 88–10–2 Cu–Ni–Fe (covered by the BS CN 102 designation [3]). Although this alloy is of comparatively low strength when compared to ferrous alloys [4] it has good corrosion resistance to flowing seawater [5] and is easily worked and welded. 90–10 copper–nickel, however, has a lower resistance to flow induced corrosion than 70–30 copper–nickel (typified by BS 2871-CN 107 [3]). Since its introduction a range of marine applications has developed for 90–10 copper–nickel where it is recommended as a high reliability-low maintenance material for pipe work, tube plates, water boxes, flanges and pump casings, in circulating systems such as condensers, heat exchangers and desalination plants [6–9]. The alloy has also been used for the sheathing of ships' hulls and offshore structures [10–13].

The main aim of this work is to inform the reader of the wide range of 90–10 copper–nickel alloy electrochemical corrosion studies. The often contradictory results and electrochemical data are concisely reviewed and throughout the paper directions are given to sources of more detailed information. Moreover, works dealing with the corrosion of copper and other copper-based alloys have been mentioned only within the context of 90–10 copper–nickel corrosion.

2. Metallurgy

A selection of national standard compositions for the general 90% copper 10% nickel alloy, wrought and cast, are given in Table 1 [14]. Copper and nickel are close in the periodic table, have a similar lattice spacing with a face centre cubic structure. The copper–nickels, therefore, form a homogeneous, α-solid solution over the complete range of Cu–Ni composition [1]. As a result of this compatibility, the physical properties of the alloy change in a smooth proportionally with increases in alloying element. Nickel increases the impact toughness, corrosion resistance and high temperature strength relative to copper.

Table 1. Selected 90–10 Cu–Ni standard compositions

Symbol /Number	National standard	Percentage composition wt/wt (range or maximum)									
		Cu	Pb	Fe	Mn	Ni	Si	S	C	Zn	Nb
CN 102	BS - wrought	Rem.	0.01	1.0–2.0	0.50–1.00	10.0–11.0	–	0.05	0.05	–	–
CuNi10Fe1Mn/ CW352H	BS EN - wrought	Rem.	–	1.0–2.0	0.5–1.0	9.0–11.0	–	–	–	–	–
CuNi10Fe1Mn-C/ CC380H	BS EN - cast	Rem.	–	1.0–1.8	1.0–1.5	9.0–11.0	–	–	–	–	–
C70600		Rem.	0.05	1.0–1.8	1.0	9.0–11.0	–	–	–	1.0	–
C70610		Rem.	0.01	1.0–2.0	0.50–1.00	10.0–11.0	–	0.05	0.05	–	–
C70620	ASTM - wrought	Rem.	0.02	1.0–1.8	1.0	9.0–11.0	–	0.02	–	0.50	–
C70690		Rem.	0.001	0.005	0.001	9.0–11.0	–	–	–	–	–
C70700		Rem.	–	0.05	0.50	9.5–10.5	–	–	–	–	–
C96200	ASTM - cast	Rem.	0.01	1.0–1.8	1.5	9.0–11.0	0.50	0.02	0.10	–	1.0
CuNi10Fe1Mn/ 2.0872CuNi10Fe	DIN - wrought	Rem.	0.3	1.0–2.0	–	9.0–11.0	–	0.05	0.05	0.5	–
G-CuNi10/ 2.0815.01	DIN - cast	Rem.	–	1.0–1.8	1.0–1.5	9–11	–	–	–	0.5	0.15–0.35

Additions of iron can dissolve in the α-phase and this alloying element has been predicted to increase the corrosion resistance via reinforcement of the passive film [1]. Although the solubility of iron is limited, larger amounts of iron can dissolve in the 90–10 copper–nickel than in the 70–30 alloy [5]. Air cooling after 30 min at an annealing temperature of 750 °C, aids the retention of iron in solid solution. Precipitation of iron-rich phases will occur if iron-containing copper–nickels are hot worked in the range 600 to 650 °C [2]. Segregation of the iron can also be encouraged by holding the alloy at 500 °C for 4 h [15]. Such iron rich phases have very small particle size (detection is difficult using ordinary X-ray or metallographic techniques), and are uniformly distributed. They increase hardness and strength but their effect on corrosion resistance is unclear [4, 5, 15].

Manganese is added for deoxidation of the melt, to improve the casting properties and to increase strength. Other minor alloying elements include tin for strength, silicon for good age hardening and lead in cast alloys to aid cutting (although levels of lead should be <0.02% wt/wt for deformable alloys and for welding).

3. General corrosion

90–10 copper–nickel is resistant to chloride, ammonia and sulfide stress corrosion cracking [16] and, like most copper alloys, has good resistance to biofouling due to the release of copper ions [17,18]. 90–10 copper–nickel has an inherent resistance to pitting and crevice corrosion in quiet seawater [19]. Pits, when they do occur, are generally shallow and broad in nature. Thus, unlike some austenitic grades of stainless steels, 90–10 copper–nickel performs well in quiet, clean seawater. General corrosion rates in non-polluted seawater range between approximately 0.01 and 0.20 mm y^{-1} (0.2 and 17.6 μA cm^{-2}) [20] where rates are higher during the earlier stages of exposure before maturation of a protective surface film [21]. These initial corrosion rates tend to be up to 30% higher under conditions of flow (0.6 m s^{-1}) than those measured in quiet seawater. In flowing seawater, the corrosion rate of 90–10 copper–nickel will decrease continually as the protective nature film continues to improve with time [21].

If the velocity of the medium is increased beyond a critical point, however, the protective film will be damaged by erosion corrosion/impingement attack and the active underlying metal will be exposed ('breakaway corrosion'). For pipe diameters >100 mm, seawater flow velocities (taken from BS MA 18:1973, 'salt water piping systems in ships') are limited to 3.0 m s^{-1} for aluminium brass, 3.5 m s^{-1} for 90–10 copper–nickel and 4.0 m s^{-1} for 70–30 copper–nickel. The critical flow velocity for enhanced attack is not only dependent on seawater velocity but also dependent on the diameter of the pipework, where smaller diameters are more aggressive due to increased wall shear stresses at equivalent bulk fluid velocities [22].

A model describing the observed limits of the flow-induced corrosion resistance of the 90–10 and 70–30 copper–nickel alloys in seawater was produced by Efird in 1977 [22]. The mechanism of passive film removal and subsequent accelerated corrosion was attributed to a susceptibility to a critical shear stress, τ_c. It was proposed that the protective layers are 'physically removed' when the shear stress at the corrosion product/seawater interface is greater than the binding force of the corrosion product film to the metal surface. The existence of this proposed, critical wall shear stress (related to the critical or breakaway velocity) at which accelerated corrosion of copper proceeds has received some confirmation by Lotz and Heitz from the description of copper erosion corrosion [23]. The work of some authors, however, has failed to determine a value of τ_c for the seawater and aqueous NaCl systems. Diem and Orazem [24] studied the effect of jet impingement in

3.5% NaCl. They found that the accelerated corrosion effect did not occur over a large range of imposed wall shear stresses including the value of 9.6 N m^{-2} proposed by Efird [21] and Lotz and Heitz [23]. Macdonald et al. [25] postulated that the critical shear stress required to physically remove the cuprous oxide corrosion product film is actually much greater than the shear stresses induced under the normal conditions of flow found in pipes.

An alternative mechanism of accelerated attack based on a mixed physical and diffusion controlled dissolution was postulated by Bianchi et al. [26]. Here, the critical mechanism of film loss is through an accelerated, chloride-facilitated dissolution of the underlying cuprous oxide (Cu_2O) semipassivating film (Reaction 1). Dissolution will occur more rapidly after the relatively nonadherent top layer of insoluble cupric species has been removed by local impingement attack.

$$Cu_2O + H_2O + 4Cl^- \rightleftharpoons 2\,CuCl_2^- + 2\,OH^- \qquad (1)$$

The semiporous cupric species at a mature film provide resistance to the diffusion of $CuCl_2^-$ and OH^- reaction products away from the lower more soluble Cu_2O film. They also resist the diffusion of corrosive chloride ions in the opposite direction towards the more vulnerable cuprous lower layers. For copper or a copper based alloy which has a mature and in-tact duplex film of corrosion products, the cuprous layer will be preserved under bulk fluid conditions where thermodynamically it would be expected to dissolve. Thus, the copper metal is protected by the cuprous oxide film, which, in turn, is protected by the insoluble cupric species. This model is appropriate where local fluid impingement under disturbed flow can produce shear stresses necessary for the removal of the upper layered cupric species rather than the more closely adhered cuprous corrosion product layer.

In addition, active–passive cell formation will develop if selective stripping of the upper protective layer occurs [26]. Dissolution of the solid cuprous species will cause bare copper alloy to become exposed and relatively active (anodic). Oxygen reduction:

$$O_2 + 2\,H_2O + 4\,e^- \rightarrow 4\,OH^- \qquad (2)$$

on the surrounding, intact cuprous oxide film (comparatively cathodic) will complete a galvanic corrosion cell which can facilitate destructive dissolution at the exposed anodic sites.

4. Passive film characteristics

In unpolluted seawater, the 90–10 copper–nickel corrosion product film is dominated by cuprous oxide and copper(II) based compounds such as atacamite ($Cu_2[OH]_3Cl$) and cupric oxide (CuO) [18]. The Cu(II) species will generally overlie the cuprous species [27, 28]. As already discussed, the protective nature of the film increases with time and is apparently much improved by the presence of nickel and iron within the film.

In seawater, the presence of sulfide has been shown to increase copper-based materials corrosion rate [29–31] and interfere with film formation to produce a nonprotective, black layer containing cuprous oxide and the sulfide ion [32–36]. Films grown/matured in unpolluted seawater, however, have been shown to be tolerant of the sulfide ion on subsequent exposure to polluted environments.

In 1952, Stewart and LaQue [5] suggested that iron in solid solution improved the overall corrosion resistance of 90–10 copper–nickel through the formation of hydrated iron oxides within the corrosion product film. Pryor et al. [37, 38] later postulated that cuprous oxide films formed on 90–10 copper–nickel provided an ohmic resistance to polarization and the corrosion reaction. A defect structural model was proposed where the improved corrosion resistance of copper–nickel–iron alloys relative to copper is due to an overall increased resistivity of the cuprous oxide film. In this model, alloying additions present in solid solution with copper, do not form oxides distinct from the base metal oxide but enter and modify the semiconducting properties of the cuprous oxide lattice. A rise in ionic and electronic resistivity with nickel and/or iron additions was said to be due to a net reduction of cation vacancies as the high valency alloying cations enter the Cu_2O lattice. Comparative resistivities of cuprous oxide films formed in boiling NaCl solution supporting this inference are shown in Table 2. As the percentage of alloyed nickel is increased from 0 to 30% wt/wt, the film resistivities increase in sympathy. The higher the valency of the alloying element the greater the number of cation vacancies and positive holes neutralized.

As noted by Burleigh and Waldeck [39] the primary assumption of the theory of North and Pryor [38] contradicts the generally accepted view that the introduction of cations of increasing valency will increase the ionic conductivity of p-type semiconductors such as Cu_2O; NiO and Fe_2O_3. These species will act as n-type dopants. Burleigh and Waldeck proposed that the reduction of corrosion rate could have been related only to the decrease in positive holes resulting in a decreased electrical conductivity. Their conclusion was that the corrosion rate is only sensitive to the magnitude of electronic transfer through the film.

Table 2. Resistivities of cuprous oxide films formed over 30 days free corrosion in boiling NaCl solution, after North and Pryor [38]

Metal	Resistivity /$\mu\Omega$ cm^{-1}	
	Electronic	Ionic
Pure copper	200	140
90–10 copper–nickel	530	250
70–30 copper–nickel	2360	600

Bockris et al. [40] examined the individual dissolution rates of copper and nickel as a function of potential and alloy composition. The rate constants for the dissolution of individual components were predicted to be independent of alloy composition and equal to that of the pure copper, nickel or iron component dissolving from its lattice. For 10% nickel, a single surface phase of copper products would dominate. Above 45% nickel at the surface of the metal it was suggested that a nickel reaction product phase would form as one component of at least two distinct surface phases.

Blundy and Pryor [37] anodically polarized 90–10 copper–nickel in 0.5 mol dm^{-3} NaCl and observed a potential dependence on the concentration of nickel in the resulting insoluble corrosion product film. Their results showed that under polarization conditions very close to open circuit potential (OCP) the reaction products contain nickel concentrations in excess of those in the metal. At more positive overpotentials (e.g., 0.0 V vs SCE), however, the trend was reversed.

Popplewell et al. [15] examined the corrosion films of 90–10 copper–nickel (grown 'naturally' at OCP) in 3.4% wt/vol NaCl with varying metallic iron concentrations from 0.03 to 1.54% wt/wt. Comparison was also made between alloys with precipitated iron phases and those with iron in solid solution. For the former case, a complex iron corrosion product, which grew over a cuprous oxide film, was proposed to be responsible for an increased corrosion resistance of the alloy. The iron products were said to be produced through preferential dissolution of the iron rich phase in the alloy. For 90–10 copper–nickel alloys with the iron in solid solution, such a discreet iron corrosion product was observed within the film layering. A model, which incorporated modification of the cuprous oxide film similar to that proposed by North and Pryor [38]), was adopted. Popplewell et al. noted that there was an increase in film electronic resistance with no impact on ionic resistance. Large quantities of nickel were observed within the cuprous oxide film in both cases, especially close to the metal surface (up to 30% wt/wt). Larger concentrations of this form of nickel were found with the precipitated iron phase alloy.

Efird [22] carried out corrosion tests on alloys of varying nickel and iron content in both quiet and rapidly flowing seawater. In the absence of iron, there was excess oxygen and little nickel in the cuprous oxide layer. When iron was present, nickel enrichment occurred but the form of the nickel depended on whether or not the iron was in solid solution. With iron in solution, there was an excess of nickel in the film (apparently present in the unoxidized state). Here the films were brown in colour. When the iron was largely precipitated out of solid solution, there was excess oxygen in the film the nickel was present as oxide and the films were black.

MacDonald et al. [25] showed that the main constituents of 90–10 copper–nickel corrosion product films formed after exposure to flowing seawater were copper, nickel, oxygen and chlorine. This indicated the presence of hydroxy chlorides as well as oxides (the ratio of copper to nickel in the corrosion product was lower than that in the alloy). Ijsseling et al. [41] found that after one week exposure of 90–10 copper–nickel in seawater, there was a slight accumulation of iron and nickel within the corrosion product at the metal–film interface. The quantity of these species increased substantially after 6–8 weeks of exposure.

Schrader [42] proposed a mechanism of film growth on 90–10 copper–nickel in seawater, which included the formation of an iron rich layer in the form of an oxide or hydroxide. Such a film formed over the alloy surface within the first few weeks of exposure. Copper and nickel rich corrosion products were then proposed to grow over the initial iron oxide/hydroxide layer. Iron in the alloy appeared to oxidize preferentially due to its more base character to produce a barrier to the diffusion of oxygen and the chloride ion. In a similar study by Chauhan and Gadiyar [43], iron oxide was not detected in corrosion product films formed at the alloy in a synthetic seawater. The inner layer of the corrosion product revealed mainly cuprous oxide containing chloride ions and nickel ions in the two valence states of Ni^{2+} and Ni^{3+}. The possibility that the nickel ions could be acting as a dopant within the cuprous oxide was acknowledged but the simultaneous presence of a separate nickel oxide (Ni_2O_3) was also not ruled out.

5. Polarization behaviour

In their 1970 paper, North and Pryor [38] investigated the anodic polarization of 90–10 copper–nickel in 0.5 mol dm^{-3} NaCl. They used linear sweep voltammetry (LSV) to produce curves with an initial peak followed by a distinct potential region of limiting current density. This behaviour was very similar to the typical curves measured on unalloyed copper [44–46]. The peak was dependent on the potential sweep rate and disappeared at very low values of sweep rate (values not specified in the original work). A schematic of the typical anodic polarization response for this system is given in Figure 1.

The anodic polarization behaviour of a 90–10 copper–nickel with 1.21% iron was also investigated by Giuliani et al. [47] where again the response was similar to that of pure copper. In 0.44 mol dm^{-3} NaCl solution the tests revealed that voltammetric slopes within an 'apparent Tafel' region close to the OCP are sensitive to electrolyte velocity. Within this region higher current densities were measured at greater electrode rotation rates. For the rotating disc electrode (RDE) the anodic slope, β_A, within this apparent Tafel region can be described via Equation 3 [48].

$$\frac{\mathrm{d}\log(\mathrm{d}i^{-1}/\mathrm{d}\omega^{-0.5})}{\mathrm{d}E} = \frac{-zF}{2.3RT} = \beta_A = 1/(59\,\mathrm{mV\,decade^{-1}}) \quad (3)$$

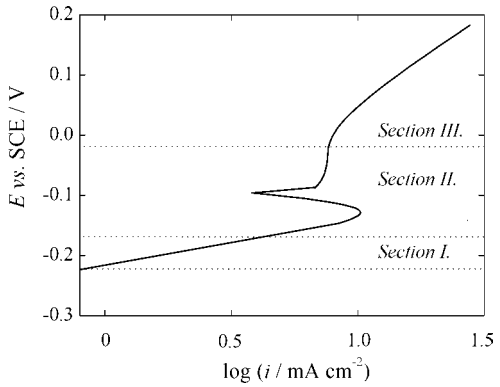

Fig. 1. A typical response to the anodic polarization of 90–10 copper–nickel in chloride media. Section I: apparent Tafel region, Section II: peak maximum and subsequent limiting current density and Section III: production of Cu(II) species at more positive overpotentials.

where, ω, z, F, R and T are the angular velocity, number of electrons involved in the mass transport limited reaction, the Faraday constant, the molar gas constant and the absolute temperature, respectively. It should be noted that in the literature, the charge transfer coefficient for the anodic response, α_A, is usually omitted from this version of the standard Tafel equation in order to provide a slope of about1/60 mV decade^{-1} for a single exchange of an electron. Further work by Kear [49] was able to reproduce the apparent Tafel response at low anodic overpotentials (Figure 2) as a function of both RDE and rotating cylinder electrode (RCE) angular velocity. In the following review of the anodic literature the anodic reaction universally taken to be under a form of mixed charge and mass transfer control where an 'apparent' Tafel slope refers to a linear response superficially similar to that of a 'true' Tafel slope.

Giuliani, Tamba and Modena [47] also used LSV to reproduce the passivation peak (−0.010 V vs SCE) and the region of limiting current density. For the applied electrodissolution of 90–10 copper–nickel and the subsequent growth of a passive film, the production

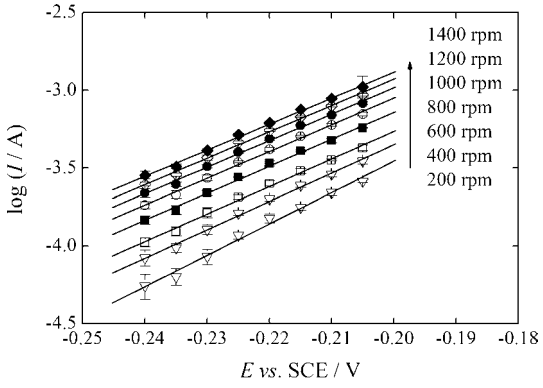

Fig. 2. 'Apparent' Tafel slopes for the electrodissolution of 90–10 copper–nickel in filtered seawater as a function of mass transfer conditions at a 20 mm diameter rotating cylinder electrode.

the free cuprous ion was chosen as the initial anodic step (Reaction 4). This was followed by combination with a chloride ion to produce solid cuprous chloride (Reaction 5):

$$\mathrm{Cu} \underset{k_{-1}}{\overset{k_1}{\rightleftharpoons}} \mathrm{Cu^+} + 1\,\mathrm{e^-} \tag{4}$$

$$\mathrm{Cu^+} + \mathrm{Cl^-} \underset{k_{-2}}{\overset{k_2}{\rightleftharpoons}} \mathrm{CuCl} \tag{5}$$

After deposition of cuprous chloride at the alloy surface the deposit is hydrolysed to give the more thermodynamically stable cuprous oxide:

$$2\,\mathrm{CuCl} + \mathrm{H_2O} \underset{k_{-3}}{\overset{k_3}{\rightleftharpoons}} 2\,\mathrm{Cu_2O} + 2\,\mathrm{HCl} \tag{6}$$

Further dissolution of the alloy at potentials more positive than the passivation peak was accepted to occur via the solid state formation of cuprous oxide. Selective dissolution of alloying elements was considered but the alloy behaviour could not be represented by a simple linear combination of two partial currents for copper and nickel dissolution. On analysis of the artificially produced corrosion product film, neither separate nickel/iron oxide/hydroxide phases or NiO enrichment of the cuprous oxide were observed.

A further study of the electrodissolution of a 90–10 copper–nickel RDE in acid chloride by Walton and Brook [50] produced similar results to Giuliani et al. Close to the OCP, alloy dissolution appeared to occur via the simple dissolution of the copper component. The alloy was thought to dissolve initially through the solid state formation of cuprous chloride (Reactions 7 and 8):

$$\mathrm{Cu} + \mathrm{Cl^-} \underset{k_{-4}}{\overset{k_4}{\rightleftharpoons}} \mathrm{CuCl} + 1\,\mathrm{e^-} \tag{7}$$

$$\mathrm{CuCl} + \mathrm{Cl^-} \underset{k_{-5}}{\overset{k_5}{\rightleftharpoons}} \mathrm{CuCl_2^-} \tag{8}$$

At low positive overpotentials, the reaction was assumed to be partially controlled by the mass transport of $CuCl_2^-$ from the dissolving CuCl at the electrode surface (also observed by other workers for unalloyed copper in chloride media [51]). The Koutecky–Levich relationship was used to produce anodic Tafel slopes for pure charge transfer controlled current (0.091 V decade^{-1}) limited by a single electron transfer. In agreement with prior authors, passivation peaks and limiting current densities were again observed at more positive overpotentials. Within this region, the currents were attributed to the production and dissolution of CuCl (the most thermodynamically stable, solid cuprous species in acid solution). The Levich relationship for the RDE (Equation 9) was used to describe the reaction

where the rate is determined only by the rate of transport of the soluble reaction product;

$$i_L = 0.62\, zFD_{CuCl_2^-}^{0.667} v^{-0.167} \omega^{0.5} [CuCl_2^-] \quad (9)$$

where i_L, D and v are the limiting current density, the diffusion coefficient and the kinematic viscosity of the solution. The linear dependence of the limiting current density measured by Walton and Brook on the square root of rotating disc electrode angular velocity was said to be poor, which from Equation 9, indicated a lack of pure mass transfer control over the reaction rate. The reader should be aware that direct comparison of results obtained in acid solution with neutral solution may not be appropriate.

Kato et al. [19, 52] studied the cathodic and anodic polarization characteristics of 90–10 copper–nickel before and after an exposure time of 191 days in 0.5 mol dm^{-3} NaCl. It was shown, via derivation of the mixed (corrosion) potential, that a decrease in corrosion rate observed during the exposure period was mainly due to a decrease in the rate of oxygen reduction rather than a less significant inhibition of the anodic reaction. Oxygen reduction was found to occur mainly at a thin, strongly adherent inner layer (the identity of which was not specified). This layer was assumed to be in contact with the electrolyte through pores in a relatively thick outer surface layer. The rate of electron transport through the inner layer determined the corrosion rate of the metal with a mature film. The anodic polarization curves were similar again to that of pure copper and the morphology showed definite potential sweep rate dependence. Current densities at anodic overpotentials decreased markedly at surfaces where the films were grown over increasing times of exposure. The direct dissolution of the copper in the alloy to the cuprous dichloride complex (Reaction 10) was assumed, which was thought to be under some form of mass transport control within the potential region of apparent Tafel behaviour:

$$Cu + 2\,Cl^- \underset{k_{-6}}{\overset{k_6}{\rightleftharpoons}} CuCl_2^- + 1\,e^- \quad (10)$$

In contrast to the less reproducible work of Walton and Brook [50], Kato and Pickering [52] found that plots of anodic limiting current density vs. the square root of RDE angular velocity were linear and passed directly through the origin, thus indicating full mass transport control of the dissolution reaction at these overpotentials. Kato et al. [19] also showed that the use of buffers significantly affected the anodic polarization response of the 90–10 copper–nickel alloy. With borate (pH 8.00) and phosphate (pH 7.88) buffers, limiting current densities were an order of magnitude lower than those measured in unbuffered electrolyte (pH 8–10). The apparent Tafel region, however, remained unaffected by the pH change. Both current densities measured in the apparent Tafel and limiting regions were higher in an ammonia buffer (pH 8–10) than those measured within buffer free solution.

Schiffrin and de Sanchez [48] adopted the dissolution of copper to the free cuprous ion (shown in Reaction 4) to describe the anodic behaviour of 90–10 copper–nickel in chloride solution. For a freshly polished surface, this reaction was again assumed to be under some form of mass transport control. Anodic Tafel slopes of 60 mV $decade^{-1}$ were said to correspond to $\alpha_A = 0$ and $z = 1$. Due to the uncertainties in the determination of z and α_A, any codissolution of the alloying elements could not be detected at low anodic overpotentials and only cuprous products were detected within the anodic limiting current region. This indicated that the dissolution reaction was nonselective throughout. In agreement with Walton and Brook [50], the dissolution rate was also found to be under full mass transport control at the limiting current. At potentials more positive than the limiting current region, however, copper/cuprous species were actively oxidized to cupric species.

The authors also determined that the overall effect of an increased concentration of chloride ions was to magnify the anodic currents both within the apparent Tafel region and the limiting current region. A tenfold increase in current was observed within the apparent Tafel region for an increase in chloride concentration from 0.1 to 0.7 mol dm^{-3}. Above 4.0 mol dm^{-3} chloride ion concentration, the peak maximum was no longer observed.

Kear [49] found that, over a RDE rotation range of 200 to 9500 rpm the morphology of anodic LSV curves closely followed those independently measured at copper (Figure 3). For all of the plots, the limiting current density at each rotation rate was dependent on the electronic resistance and chemical dissolution properties of a surface film which, in turn, were dependent on the rate of mass transport of dissolution products from the electrode–electrolyte interface. This was inferred from analysis of the relatively large peak current densities in comparison to the limiting current density values. Unalloyed copper showed no such peak at higher rotation rates indicating the absence of an insulating

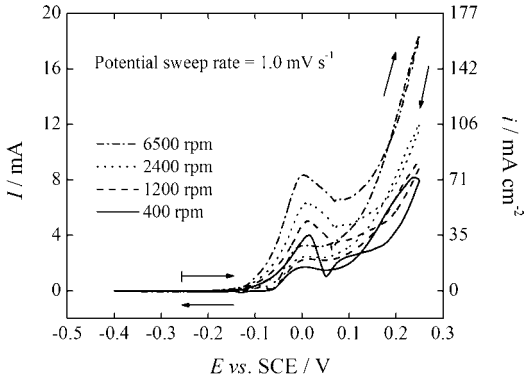

Fig. 3. Cyclic voltammetry at the 90–10 copper–nickel RDE (OCP → anodic → cathodic → OCP) as a function of RDE rotation rate in filtered seawater.

surface film. The measured limiting current density reached steady state limit at about + 0.09 V vs SCE where the magnitude of the current corresponded to the rate of mass transport of $CuCl_2^-$ from the electrode surface after film dissolution. From this work, it is clear that the 90–10 copper–nickel film was much less soluble and, therefore, more protective than the film formed at pure copper under the same conditions.

Ceré et al. [53] studied the reduction of hydrogen peroxide on 90–10 copper–nickel in 0.1 mol dm^{-3} borax buffer solution. The reduction reaction took place on a surface mainly composed of cuprous oxide. It was proposed that Cu_2O is catalytic to peroxide reduction via the surface redox couple Cu(I)/Cu(II):

$$Cu^+ + H_2O_2 \rightarrow Cu^{2+} + OH^- + OH\cdot \quad (11)$$

$$Cu^+ + OH\cdot \rightarrow Cu^{2+} + OH^- \quad (12)$$

This is an electrochemical–chemical reduction mechanism that was very similar to that proposed by the same authors for the reduction of hydrogen peroxide and oxygen at pure copper [54, 55]. The catalytic reduction of peroxide at 90–10 copper–nickel appears to directly emulate that which occurs on unalloyed copper [54, 56, 57] where surface corrosion products in each case influenced the rate of oxygen reduction where cuprous and cupric species acted to catalyse or slow the kinetics of oxygen reduction, respectively.

For freshly polished surfaces single mass transfer limited waves (see Figure 4 for typical examples [49]) were observed indicating a lack of hydrogen peroxide build up during the reduction sequence (due to catalytic decomposition of the intermediate). Reviews of literature cathodic and anodic Tafel slopes measured for the 90–10 copper–nickel alloy in chloride media are given in Tables 3 and 4 for a range of experimental conditions.

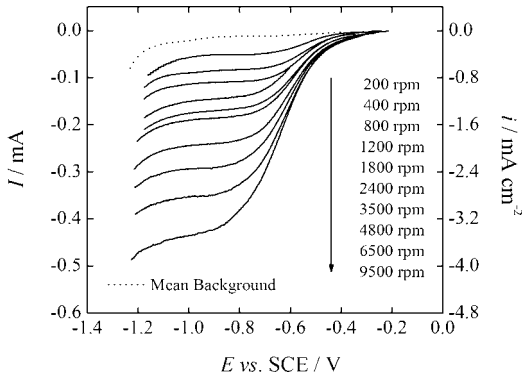

Fig. 4. Oxygen reduction at a 90–10 copper–nickel RDE in aerated filtered seawater measured at a potential scan rate of 0.5 mV s^{-1}.

6. Corrosion mechanism

The flow-enhanced corrosion mechanism of 90–10 copper–nickel in seawater, with and without sulfide contamination, has been investigated by de Sanchez and Schiffrin [48]. The mixed potential was derived using the current vs potential response from pure charge transfer controlled oxygen reduction and apparent Tafel slopes for the mass transport controlled electrodissolution of the copper component of the alloy. A representation of the mixed potential derivation process is given in Figure 5 for two differing rates of mass transfer (proportional to ω). It is clear from this Figure that higher fluid velocities produce greater corrosion rates and more negative corrosion potentials due to an accelerated rate of the anodic reaction. Expressions were presented for the derivation of the corrosion current density and the corrosion current. This approach was similar to that adopted in earlier work on pure copper in chloride by Faita et al. [65]. The corrosion rate of freshly polished 90–10 copper–nickel in seawater was estimated to be 12 μA cm^{-2}. This value dropped to 5 μA cm^{-2} after natural ageing in a nonstatic electrolyte over 20–22 h.

Table 3. Review of cathodic Tafel slopes for 90–10 copper–nickel in aerated chloride media

Electrolyte	T / °C	Surface condition	β_C /V $decade^{-1}$	Ref.
Seawater	20	freshly polished	−0.120 to −0.150	[48]
0.5 mol dm^{-3} NaCl* and artificial seawater†	25	freshly polished	−0.187 (1000 rpm)* −0.180 (1000 rpm)† −0.203 (1600 rpm)* −0.200 (1600 rpm)† −0.185 (2500 rpm)* −0.175 (2500 rpm)† −0.173 (3000 rpm)* −0.175 (3600 rpm)† −0.161 (3600 rpm)* −0.189 (5000 rpm)† −0.167 (5000 rpm)* All slopes ± 0.005 −0.187 (6000 rpm)*	[58]
Natural seawater	20	freshly polished	−0.346	[59]
Natural seawater	20	freshly polished	−0.052	[60]
Natural and artificial† seawaters	–	freshly polished‡ 75 days exposure§	−0.230‡ −0.090†‡ −0.040§ −0.100†§	[61]
Aerated artificial seawater	–	freshly polished	−0.108	[62]
Aerated filtered and artificial seawaters†	25	freshly polished	RDE −0.167 to −0.203 and −0.168 to −0.181† RCE −0.141	[49]

*, †, ‡ and § denote 0.5 mol dm^{-3} aqueous NaCl, artificial seawater, freshly polished and aged surfaces, respectively.

Table 4. A review of directly measured anodic apparent Tafel slopes for 90–10 copper–nickel in neutral 3.0%–3.5% NaCl and natural and artificial seawaters (RRDE refers to the rotating ring disc electrode)

Electrolyte	Geometry	T / °C	Surface condition	β_A /V decade^{-1}	Ref.
Aerated HCl	static	27–70	freshly polished	0.130 ± 0.008	[40]
Aerated HCl	RDE	–	freshly polished	0.072 to 0.091	[50]
Aerated NaCl	static	23 ± 3	freshly polished[†]	0.070[‡]	[19]
			exposed at OCP[§]	0.075 (5 days exposure) [§] 0.100 (10 days exposure) [§] 0.110 (15 days exposure)[§] 0.120 (191 days exposure)[§]	
Aerated seawater	RDE	20 ± 1	freshly polished	0.060	[48]
Aerated NaCl	RDE	23 ± 3	freshly polished	0.060 to 0.062 (−0.267 to −0.190 V vs SCE) 0.070 to 170 (−0.170 to −0.070 V vs SCE)	[51]
Deaerated HCl	RRDE	23	freshly polished	0.070 (700 rpm)	[63]
0.5 mol dm^{-3} NaCl* and artificial seawater[†]	RDE	25	freshly polished	$0.059^{*}_{(1000\text{rpm})}$ $0.045^{\dagger}_{(1000\text{ rpm})}$ $0.054^{*}_{(1600\text{ rpm})}$ $0.047^{\dagger}_{(1600\text{ rpm})}$ $0.045^{*}_{(2500\text{ rpm})}$ $0.046^{\dagger}_{(2500\text{ rpm})}$ $0.062^{*}_{(3000\text{ rpm})}$ $0.061^{\dagger}_{(3600\text{ rpm})}$ $0.052^{*}_{(3600\text{ rpm})}$ $0.048^{\dagger}_{(5000\text{ rpm})}$ $0.052^{*}_{(5000\text{ rpm})}$ All slopes ± 0.005 $0.062^{*}_{(6000\text{ rpm})}$	[58]
Aerated NaCl	RDE	25	freshly polished	0.062	[64]
Aerated seawater	pipe flow	20	freshly polished	0.057	[59]
Aerated seawater	jet impingement	20	freshly polished	0.055	[60]
Aerated natural and artificial[†] seawaters	static	–	freshly polished[‡]	0.050[‡] 0.054[†‡]	[61]
			75 days exposure[§]	0.030[§] 0.050[†§]	
Aerated artificial seawater	static	–	freshly polished	0.045	[62]
Aerated filtered and artificial[†] seawaters	RDE and RCE	25	freshly polished	0.065 to 0.069 0.066 to 0.070 0.049 to 0.057	[49]

*, [†], [‡] and [§] denote 0.5 mol dm^{-3} aqueous NaCl, artificial seawater, freshly polished surfaces and aged surfaces, respectively.

Expressions describing corrosion current density and the corrosion potential as a function of RDE rotation rate were also developed by Dhar et al. [66]. They assumed that selective corrosion of the copper in the 90–10 copper–nickel alloy occurred via the cuprous dichloride complex according to the reversible, mechanism described in Reaction 10. The cathodic process was taken as irreversible but limited to the two-electron reduction of oxygen to peroxide:

$$O_2 + 2\,H_2O + 2\,e^- \rightarrow H_2O_2 + 2\,OH^- \qquad (13)$$

Calculated changes in the value of the corrosion potential as a function of logarithmic rotation rate (rpm) for the 90–10 copper–nickel were −0.021 and −0.026 V decade^{-1} for NaCl and artificial seawater, respectively. Corrosion current densities varied from about 9–13 μA cm^{-2} and 16 to 21 μA cm^{-2} in the seawater and the NaCl solution, respectively. The higher corrosion rates in the 0.5 mol dm^{-3} NaCl was attributed to the lower buffering capacity of this electrolyte. Table 5 summarises published corrosion rate data for freshly-polished 90–10 copper–nickel where mean electrodissolution rates can range between 0.5 to 21 μA cm^{-2} (0.01–0.24 mm y^{-1}). It should be noted that pure charge transfer control of the 90–10 copper–nickel corrosion rate in assumed in all of these works, but it may be possible that film formation at the alloy could reduce the rate of species mass transport to levels at which may influence the rate of either the cathodic or anodic reactions [67].

7. Linear polarization resistance (LPR)

Several studies have also been performed using polarization resistance, R_p in conjunction with the Stern–Geary relationship [68]:

$$i_{corr} = \frac{\beta_A \beta_C}{2.3 R_p (\beta_A + \beta_C)} = \frac{B}{R_p} \qquad (14)$$

The mixed charge and mass transport controlled, apparent Tafel slopes for the anodic reaction are usually taken as β_A. A review of literature proportionality constants, B, for the corrosion of 90–10 copper–nickel in

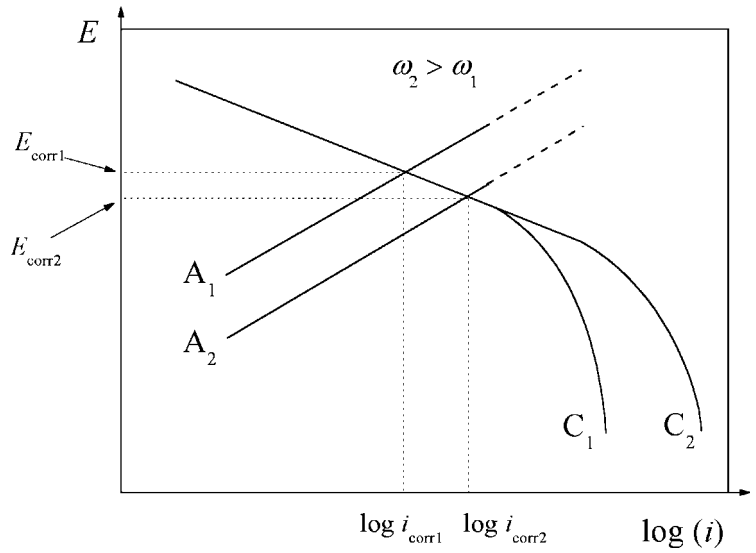

Fig. 5. Schematic describing the derivation of the mixed/corrosion potential from the extrapolation of measured polarization curves in aerated chloride media for two differing mass transfer conditions, ω_1 and ω_2. Anodic and cathodic polarization curves are represented by A_x and C_x, respectively.

Table 5. Freshly polished 90–10 copper–nickel corrosion rates in unpolluted, aerated seawaters assuming 1 mm $y^{-1} \simeq 86$ μA cm^{-2}

Reference	[48]	[59]	[71]	[33]	[66]	[62]
mm y^{-1}	0.06–0.13	0.07	0.18	0.05	0.10–0.24	0.01
μA cm^{-2}	5.2–11.2	5.9	15.2	4.16	9–21	0.52

chloride media is given in Table 6. Only charge transfer controlled data can be used to derive Tafel slopes and, therefore, a correct value of corrosion current via the Stern–Geary equation. This relationship has been frequently abused under industrial and academic conditions in the case of copper-based materials because, in all cases, reasonable values of Tafel slope produce very similar results. It is the value of inverse polarization resistance which provides the true indication of corrosion rate. Values of B are published, however, and range widely from 0.016–0.070 V. Syrett and MacDonald [74] examined the validity of electrochemical methods (LPR, potential step and a.c. impedance techniques) for the measurement of the corrosion rates of copper–nickel alloys (including 90–10 copper–nickel) in seawater. Values of the corrosion rate, derived via the Stern–Geary relationship at various oxygen concentrations, compared very well with weight loss data measured over extended time periods. Discrepancies between electrochemical and traditional corrosion rates were attributed to the very high rates of initial dissolution immediately after immersion. For a dissolved oxygen concentration of 6.6 ppm, inverse resistance polarization measurements at 90–10 copper–nickel began at 8 $k\Omega^{-1}$ (0.7 $k\Omega^{-1}$ cm^{-2}) and rapidly decreased to about 2 $k\Omega^{-1}$ (0.2 $k\Omega^{-1}$ cm^{-2}) over a 120 h period.

Table 6. Values of the proportionality constant, B, in the Stern–Geary equation

Electrolyte(s)	B / V $decade^{-1}$	Ref.
Natural seawater	0.040–0.107	[28]
Natural seawater	0.018	[48]
Natural and artificial† seawaters	0.016–0.023 and 0.019–0.028†	[49]
3.5% NaCl* and natural seawaters	0.018* and 0.016	[58]
Natural seawater	0.034	[59]
Natural and artificial† seawaters	0.014–0.019†	[61]
Natural and Artificial† seawaters	0.049–0.018†	[69]
Natural seawater	0.049‡	[70]
Natural seawater	0.018‡	[71]
Natural seawater	0.070	[72]
Natural seawater	0.021	[73]

* and † denote aqueous NaCl and artificial seawaters, respectively.
‡ As quoted by Callow et al. [69].

The corrosion of 90–10 copper–nickel in seawater was also investigated by Mansfeld et al. [61] using LPR with the rotating cylinder electrode. The four-electron reduction of oxygen was taken as the cathodic reaction. The electrodissolution of the copper in the alloy was assumed to occur via the free cuprous ion, according to Reaction 4. The cuprous ion is subsequently complexed by the chloride ion to give a cuprous dichloride complex. It was concluded that mass transport of either the chloride ion to the electrode surface or mass transport of the cuprous dichloride complex away from the surface (neither was specified) was the rate-determining step of the anodic reaction and the overall corrosion reaction. It was found that the corrosion potential, E_{corr}, did not change significantly with

increasing rotation rate but $1/R_p$ increased linearly with rotation rate, r (rpm), to the power 0.7. It is clear from this work, however, that the relationships displayed limited linear characteristics. Equations 15 and 16 are the empirical expressions derived for, E_{corr} (mV vs SCE) and $1/R_p$ (Ω^{-1} cm^{-2}), respectively.

$$E_{corr} = a_1 + a_2 \times r_{(rpm)}^{0.7} \quad (15)$$

$$1/R_p = b_1 + b_2 \times r_{(rpm)}^{0.7} \quad (16)$$

For 90–10 copper–nickel, values of a_1 and a_2 were given as −299 and +0.02 mV vs SCE, respectively. Values of b_1 and b_2 were quoted as 7.2×10^{-4} and 3.3×10^{-6} Ω^{-1} cm^{-2}, respectively. After initial exposure of 90–10 copper–nickel, the LPR derived corrosion rates decreased continuously over a 30 day exposure period to reach 2.5 μm y^{-1} (0.2 μA cm^{-2}) in natural seawater and 6.0 μm y^{-1} (0.5 μA cm^{-2}) in artificial seawater. In the natural seawater, average weight loss and LPR derived values for the same period were 15.2 μm y^{-1} (1.3 μA cm^{-2}) and 7.9 μm y^{-1} (0.7 μA cm^{-2}), respectively. Equivalent values of 9.4 μm y^{-1} (0.8 μA cm^{-2}) and 14.2 μm y^{-1} (1.2 μA cm^{-2}), respectively, were measured in the artificial seawater. The overall corrosion rate of 90–10 copper–nickel was found to agree with the time law relationship

$$\text{Corrosion rate} = k_{corr} \times t^n \quad (17)$$

In natural seawater, k_{corr} equalled 117.5 μm y^{-1} (10.1 μA cm^{-2}) and the power 'n' was –0.58. For the artificial seawater, k_{corr} was 138.0 μm y^{-1} (11.9 μA cm^{-2}) and the time exponent, 'n' was given as −0.79.

8. Conclusions

The electrochemical literature on polished 90–10 copper–nickel in either seawater or sodium chloride electrolytes reveals a corrosion mechanism very similar to that of unalloyed copper. At potentials close to the corrosion potential the anodic reaction is under mixed charge transfer and mass transport controlling kinetics. The mass transport-limiting step with the anodic reaction is generally assumed to be the rate of movement of a cuprous chloride complex away from the electrode surface to the bulk of the electrolyte. The cathodic reaction is dominated by the irreversible reduction of oxygen, which remains under complete charge transfer control at potentials close to the corrosion potential. At the mixed potential, therefore, the corrosion rate will be dependent on the ambient mass transport conditions via the anodic reaction. The presence of progressively thicker surface films, however, will act to reduce the rate of both charge transfer process. Moreover, an ageing surface will also reduce the influence of bulk fluid mass transport on the polarization characteristics of the alloy.

Acknowledgements

The authors are grateful to DSTL-Farnborough (UK) and QinetQ-Haslar (UK) for financial contributions to the research programme.

References

1. R.W. Cahn, P. Hassen and E.J. Kramer, 'Materials Science and Technology, A Comprehensive Treatment, Vol. 8, Structure and Properties of Non-Ferrous Alloys' (VCH, New York, 1996).
2. T.H. Rogers, 'Marine Corrosion' (George Newnes Ltd, London, 1968).
3. British Standard BS 2871 Part 3: Copper and copper alloy tube for heat exchangers and condensers (British Standards institution, London, 1972).
4. S.H. Lo, W.M. Gibbon and R.S. Hollingshead, *J. Mater. Sci.* **22** (1987) 3293.
5. W.C. Stewart and F.L. LaQue, *Corrosion* **8** (1952) 259.
6. L. Kenworthy, *Trans. Inst. Marine Eng.* **77** (1965) 149.
7. B. Todd, 'Marine Applications of Copper–Nickel Alloys, Section 2: Materials Selection for High Reliability Seawater Systems', Technical Report (Copper Development Association, Potters Bar, UK, 1998).
8. A Working Party Report: 'Illustrated Case Histories of Marine Corrosion' (The Institute of Metals, London, 1990).
9. B. Todd and P.A. Lovett, 'Marine Engineering Practice: Selecting Materials for Sea Water Systems' Technical Report (Institute of Marine Engineers, London, 1974).
10. H.S. Campbell, 'Resistance of 90/10 Copper/Nickel Boat Sheathing and Fish Cage Mesh to Fouling and Corrosion', Dissertation (University of Surrey, Guildford, UK, 1995).
11. P.T. Gilbert, 'Use of Copper–Nickel Alloy Sheathing for Corrosion and Fouling Protection of Marine Structures,' Proceedings of the Institute of Metals Conference on Marine Engineering with Copper–Nickel, London, UK, 19–20 April (1988) pp. 21–41.
12. D.T. Peters, 'Marine Applications of Copper–Nickel Alloys, Section 5: Review of Copper–Nickel Alloy Sheathing of Ship Hulls and Offshore Structures', Technical Report (Copper Development Association, Potters Bar, UK, 1998).
13. T.J. Glover and B.B. Moreton, 'Corrosion and fouling resistance of cupro-nickel in marine environments', Proceedings of the UK National Corrosion Conference, Birmingham, UK, 16–18 Nov. (1982) pp. 105–108.
14. 'Copper Development Association Publication No. 130, Comparison of National Standards (ASTM, DIN, EN, BSI) for Copper Alloy Compositions', Technical Report (Copper Development Association, Potters Bar, UK, 1998).
15. J.M. Popplewell, R.J. Hart and J.A. Ford, *Corros. Sci.* **13** (1973) 295.
16. C.A. Powell, 'Marine Applications of Copper–Nickel Alloys, Section 1: Copper–Nickel Alloys – Resistance to Corrosion and Biofouling', Technical Report (Copper Development Association, Potters Bar, UK, 1998).
17. F.B. Mansfeld and B.J. Little, *Electrochim. Acta* **37** (1992) 2291.
18. A. Hall and A.J.M. Baker, *J. Mater. Sci.* **20** (1985) 1111.
19. C. Kato, B.G. Ateya, J.E. Castle and H.W. Pickering, *J. Electrochem. Soc.* **127** (1980) 1890.
20. 'Copper–Nickel Alloys: Properties and Applications', Technical Report (Copper Development Association, Potters Bar, UK, 1982).
21. K.D. Efird and D.B. Anderson, *Mater. Perform.* **14** (1975) 37.

22. K.D. Efird, *Corrosion* **33** (1977) 3.
23. U. Lotz and E Heitz, *Mater. Corros.* **34** (1983) 454.
24. C.B. Diem and M.E. Orazem, *Corrosion* **50** (1994) 290.
25. D.D. Macdonald, B.C. Syrett and S.S. Wing, *Corrosion* **34** (1978) 289.
26. G. Bianchi, G. Fiori, P. Longhi and F. Mazza, *Corrosion* **34** (1978) 396.
27. B.J. Little, P. Wagner and F.B. Mansfeld, *Int. Mater. Rev.* **36** (1991) 253.
28. A.H. Tuthill, *Mater. Perform.* **26** (1987) 12.
29. S.A. Campbell, G.W.J. Radford, C.D.S. Tuck and B.D. Barker, *Corrosion* **58** (2002) 57.
30. C.A. Powell, I. Penegar and S.A. Campbell, 'Copper nickel – An alternative antifoulant', Proceedings of Costings *vs* Benefits of TBT-Based & Alternative Antifoulants, Malta, 4–6 Dec. (1995).
31. C.D.S. Tuck, K.C. Bendal, R.J. Gryllis, G.W.J. Radford and S.A. Campbell, 'High strength copper nickel – Optimization of mechanical strength and marine corrosion resistance for use in naval architecture and offshore oil and gas', Paper 518 Proceedings of Corrosion 96, Denver, CO, USA, 24–29 March (1996).
32. J.F. Bates and J.M. Popplewell, *Corrosion* **31** (1975) 269.
33. J.P. Gudas and H.P. Hack, *Corrosion* **35** (1979) 67.
34. E.D. Mor and A.M. Beccaria, *Brit. Corr. J.* **10** (1975) 33.
35. B.C. Syrett, *Corros. Sci.* **21** (1981) 187.
36. L.E. Eiselstein, B.C. Syrett, S.S. Wing and R.D. Caligiuri, *Corros. Sci.* **23** (1983) 223.
37. R.G. Blundy and M.J. Pryor, *Corros. Sci.* **12** (1972) 65.
38. R.F. North and M.J. Pryor, *Corros. Sci.* **10** (1970) 297.
39. T.D. Burleigh and D.H. Waldeck, *Corrosion* **55** (1999) 800.
40. J.O. Bockris, B.T. Rubin, A. Despic and B. Lovrecek, *Electrochim. Acta* **17** (1972) 973.
41. M.E. Wilms, V.J. Gadgil, J.M. Krougman and F.P. Ijsseling, *Corros. Sci.* **36** (1994) 871.
42. M.E. Schrader, *Appl. Surf. Sci.* **10** (1982) 431.
43. P.K. Chauhan and H.S. Gadiyar, *Corros. Sci.* **25** (1985) 55.
44. H. Lal and H.R. Thirsk, *J. Chem. Soc.* (1953) 2638.
45. M. Braun and K. Nobe, *J. Electrochem. Soc.* **126** (1979) 1666.
46. H.P. Lee and K. Nobe, *J. Electrochem. Soc.* **133** (1986) 2035.
47. L. Giuliani, A. Tamba and C. Modena, *Corros. Sci.* **11** (1971) 485.
48. S.R. de Sanchez and D.J. Schiffrin, *Corros. Sci.* **22** (1982) 585.
49. G. Kear, 'Electrochemical Corrosion of Marine Alloys Under Flowing Conditions', Dissertation (University of Portsmouth, United Kingdom, 2001).
50. M.E. Walton and P.A. Brook, *Corros. Sci.* **17** (1977) 317.
51. G. Kear, D. Barker and F.C. Walsh, *Corros. Sci.* **46** (2004) 109.
52. C. Kato and H.W. Pickering, *J. Electrochem. Soc.* **131** (1984) 1219.
53. S. Cere, M.V. Vazquez, S.R. de Sanchez and D.J. Schiffrin, *J. Electroanal. Chem.* **470** (1999) 31.
54. M.V. Vazquez, S.R. de Sanchez, E.J. Calvo and D.J. Schiffrin, *J. Electroanal. Chem.* **374** (1994) 179.
55. M.V. Vazquez, S.R. de Sanchez, E.J. Calvo and D.J. Schiffrin, *J. Electroanal. Chem.* **374** (1994) 189.
56. D.J. Schiffrin, The Electrochemistry of Oxygen, *in* D. Pletcher (Ed.), 'Specialist Periodical Reports: Electrochemistry' (Royal Society of Chemistry, Cambridge, UK, 1983), pp. 126–170.
57. F. King, M.J. Quin and C.D. Litke, *J. Electroanal. Chem.* **385** (1995) 45.
58. H.P. Dhar, R.E. White, G. Burnell, L.R. Cornwell, R.B. Griffin and R. Darby, *Corrosion* **41** (1985) 317.
59. J.N. Alhajji and M.R. Reda, *Corrosion* **49** (1993) 809.
60. J.N. Alhajji and M.R. Reda, *Corros. Sci.* **34** (1993) 163.
61. F.B. Mansfeld, G. Liu, H. Xiao, C.H. Tsai and B. Little, *Corros. Sci.* **36** (1994) 2063.
62. M.R. Reda and J.N. Alhajji, *Brit. Corros. J.* **30** (1995) 56.
63. H.P. Lee and K. Nobe, *J. Electrochem. Soc.* **131** (1984) 1236.
64. R. Robles and J. Genesca, *Afinidad* **48** (1991) 25.
65. G. Faita, G. Fiori and D. Salvadore, *Corros. Sci.* **15** (1975) 383.
66. H.P. Dhar, R.E. White, R. Darby, L.R. Cornwell, R.B. Griffin and G. Burnell, *Corrosion* **41** (1985) 193.
67. R.J.K. Wood, S.P. Hutton and D.J. Schiffrin, *Corros. Sci.* **30** (1990) 1177.
68. M. Stern and A.L. Geary, *J. Electrochem. Soc.* **104** (1957) 56.
69. L.M. Callow, J.A. Richardson and J.L. Dawson, *Brit. Corros. J.* **11** (1976) 123.
70. F.P. Ijsseling, *Corros. Sci.* **14** (1974) 97.
71. H. Grubitish, F. Hilbert and R. Sammer, *Mater. Corros.* **17** (1966) 760.
72. D.D. MacDonald, B.C. Syrett and S.S. Wing, *Corrosion* **35** (1979) 367.
73. M.R. Reda and J.N. Alhajji, *J. Uni. Kuwait Sci.* **20** (1993) 171.
74. B.C. Syrett and D.D. Macdonald, *Corrosion* **35** (1979) 505.